

ViG-Bias: Visually Grounded Bias Discovery and Mitigation

Badr-Eddine Marani^{1*}, Mohamed Hanini^{1*},
Nihitha Malayarukil¹, Stergios Christodoulidis¹, Maria Vakalopoulou¹, and
Enzo Ferrante^{1,2}

¹ MICS, CentraleSupélec, Université Paris-Saclay, France

² Instituto de Ciencias de la Computación, CONICET - Universidad de Buenos Aires, Argentina

Abstract. The proliferation of machine learning models in critical decision making processes has underscored the need for bias discovery and mitigation strategies. Identifying the reasons behind a biased system is not straightforward, since in many occasions they are associated with hidden spurious correlations which are not easy to spot. Standard approaches rely on bias audits performed by analyzing model performance in pre-defined subgroups of data samples, usually characterized by common attributes like gender or ethnicity when it comes to people, or other specific attributes defining semantically coherent groups of images. However, it is not always possible to know a-priori the specific attributes defining the failure modes of visual recognition systems. Recent approaches propose to discover these groups by leveraging large vision language models, which enable the extraction of cross-modal embeddings and the generation of textual descriptions to characterize the subgroups where a certain model is underperforming. In this work, we argue that incorporating visual explanations (e.g. heatmaps generated via GradCAM or other approaches) can boost the performance of such bias discovery and mitigation frameworks. To this end, we introduce Visually Grounded Bias Discovery and Mitigation (ViG-Bias), a simple yet effective technique which can be integrated to a variety of existing frameworks to improve both, discovery and mitigation performance. Our comprehensive evaluation shows that incorporating visual explanations enhances existing techniques like DOMINO, FACTS and Bias-to-Text, across several challenging datasets, including CelebA, Waterbirds, and NICO++.

Keywords: Unsupervised bias discovery · Bias mitigation · Visual explanations

1 Introduction

The increasing adoption of deep learning-based image classification models, notably in systems like facial recognition software, raises concerns related to biases

* Equal contribution

and fairness [3]. Biases in such systems can lead to unfair and discriminatory outcomes, making it crucial to identify and address their underlying causes. Unfortunately, determining on which subgroups a given system may exhibit biased behavior is not an easy task. The typical approach to detect biases consist in auditing the system with respect to pre-defined attributes (often referred as protected attributes), like gender, sex, age or ethnicity, by comparing specific fairness metrics [2]. However, attributes like sex, age, or ethnicity are not always the real causes that explain the poor performance of a given model in a particular set of data samples. For example, in face recognition, a system may systematically fail to classify people with glasses due to the fact that they were not well represented in the training set. In this case, the auditing with standard demographic attributes, may not be able to unveil the real reason of bias. In other cases, such as the classification of animals or objects, the attributes that characterize the under-performing groups may not be obvious. Spurious correlations could lead to systems that make incorrect predictions because the model has learned these false relationships from the training data [8], or predictions which are actually correct but for the wrong reasons [24]. This issue often arises when the model is trained on datasets that do not accurately represent the real-world scenarios on which it is intended to work with, or when the dataset itself contains hidden biases. Thus, discovering the failure modes and providing explanations useful to understand the real reasons behind them becomes a crucial task when designing robust and fair systems. Existing literature refers to this task as *unsupervised discovery of bias* [14], or *slice discovery* [7], in the sense that such methods aim at mining the input data for semantically meaningful subgroups (slices) on which the model performs poorly. In this context, a slice is defined as a group of data samples that share a common attribute or characteristic which is not related to the target label.

Recent studies have shown that text explanations [12] produced by multimodal large vision language models (VLMs) [6] can assist in discovering and describing subpopulations on which a model systematically underperforms, without the need for protected attribute annotations. At the same time, a different line of work [14] has qualitatively demonstrated that visual explanations [1] derived from biased models, especially for instances originating from conflicting data slices, predominantly highlight spurious features usually associated with shortcut learning. In this work, we hypothesize that, since visual explanations for biased models tend to underscore spurious correlations, they can serve as instrumental tools in informing VLMs when they are used to identify and mitigate undesired biases. To this end, we leverage the descriptive power of recent multimodal VLMs, and combine it with the capabilities of visual explanation mechanisms to uncover biases contributing to systematic failures for unknown slices in visual recognition models. Our extensive empirical evaluation highlights the advantages of the proposed method, being easily adapted to different bias discovery frameworks and boosting systematically their performance.

Contributions: Under the hypothesis that visual explanations can assist to better identify the reasons behind biased systems, here we introduce Visually

Grounded Bias Discovery and Mitigation (ViG-Bias), a simple yet effective strategy which improves the performance of existing bias discovery and mitigation methods based on multimodal embeddings. First, we provide empirical evidence showing that visual explanations of biased models usually focus on spurious correlations. Then, we leverage such explanations to direct the attention of existing bias discovery and mitigation methods towards spurious features, resulting in improved performance in both tasks. We show that ViG-Bias is general enough to be adapted to a wide range of recent methods which address these problems using cross-modal embeddings and textual explanations obtained via VLMs, like DOMINO [7], FACTS [27] and Bias-to-Text [12], systematically improving their performance on three challenging datasets.

2 Related work

Visual explanations. Visual explanations in computer vision have largely contributed to the interpretability and trustworthiness of deep learning models. They provide insights into the decision-making process of neural networks by highlighting regions within an input image that are significant for predictions. One prominent technique in this domain is Gradient-weighted Class Activation Mapping (Grad-CAM) [21]. Grad-CAM utilizes the gradients flowing into the final convolutional layer of a CNN to understand which features are most important for a particular decision. By creating a heatmap of these weighted features, Grad-CAM offers a visual representation that demonstrates how the model focuses on different parts of the image to make a decision. This method not only aids in improving model transparency but also helps in diagnosing potential reasons for misclassifications. GradCAM has previously been employed as a description mechanism to interpret failure modes in [14]. However, even though the work of Krishnakumar et al [14] shows the potential of visual explanations for this task, they mostly provide qualitative examples and do not propose an automatic approach to bias discovery and mitigation. Singla and co-workers [22] present another interesting work where they generate annotations for visual explanations of the ImageNet dataset. They released a dataset called Salient ImageNet, which provides heatmaps distinguishing between *spurious* and *core* features, where the last ones correspond to a set of visual features that are always a part of the object definition. Even though they employ human supervision to identify the visual explanations related to spurious correlations (making the process difficult to automate), this work shows that such heatmaps can actually be used to pinpoint this type of spurious attributes. Here, we plan to leverage GradCAM heatmaps as a mechanism to direct the attention of bias discovery and mitigation methods towards spurious correlations.

Automatic bias discovery using VLMs. Several recent efforts have been conducted in the identification of biased data slices using cross-modal embeddings. The DOMINO method [7] combines cross-modal embeddings and error-aware mixture models to find semantically coherent clusters of images where a given

classification system is failing. Textual descriptions derived from the cross-modal embeddings are then used to characterize the failure modes that were just discovered. A similar approach is introduced by the FACTS (First Amplify and then Slice to Discover Bias) [27] method, where the authors propose to first amplify the sources of bias in the training to ease its identification. This process is carried out in two stages. The first stage involves amplifying the bias by regularizing the model. This is achieved through regularization by specifically increasing the weight decay factor λ , which penalizes the more significant weights in the model. Regularization is a common technique used to prevent overfitting by discouraging complex models, but in this context, it serves a dual purpose: it not only helps to prevent overfitting but also forces the model to rely more on the spurious attribute by simplifying the hypothesis space. The second stage consists of identifying underperforming data segments that exhibit unique correlations by employing mixture modeling within a feature space aligned with bias, a method known as correlation-aware slicing, similar to the aforementioned DOMINO. A different approach titled Bias-to-Text (B2T) was introduced in [12]. B2T uses linguistic interpretation to identify and mitigate biases in vision models, including image classifiers. By generating linguistic descriptions of images using VLMs, B2T extracts keywords indicative of bias from the wrongly predicted examples, thereby enabling a more focused understanding and correction of prejudices within the models.

In this work, we will show how visual explanations can boost the performance of these three approaches, by helping to better focus the model’s attention on areas containing spurious features.

Bias mitigation: improving robustness to spurious correlations. Discovering conflicting slices is important, but mitigating such biases is also crucial. A common approach is based on group distributionally robust optimization (GroupDRO) [20]. GroupDRO aims to enhance model performance across different predefined groups or subpopulations in the data, based on pre-defined protected attributes like race or gender. The objective is to minimize the worst-case loss across these groups, thereby encouraging fairness and reducing disparities in model performance among them. However, one notable drawback of this technique is the requirement to assign specific group labels to every dataset entry, which can lead to substantial increases in annotation costs, and requires to know before-hand such groups. Another existing approach in the bias mitigation field is JTT (Just Train Twice) [15]. JTT starts with the standard training of the model to pinpoint examples that have been misclassified. Following this, the training process is adjusted by reweighting the dataset, giving greater importance to these previously misclassified examples. JTT forces the model to pay more attention to examples where the model is failing, thereby enhancing its performance on those specific examples. Here, we will employ JTT as a baseline approach for comparison, and propose ways to integrate visual explanations into the group definitions for GroupDRO.

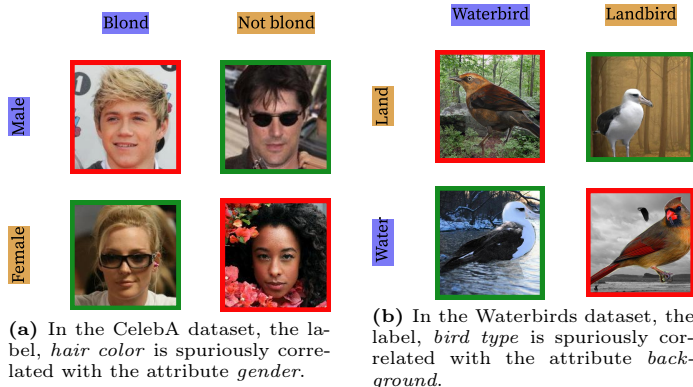


Fig. 1: The four groups in the CelebA (left) and Waterbirds (right) datasets are based on combinations of the spurious attribute and the label. The groups highlighted in green have the most training samples, whereas the groups highlighted in red have the least training samples.

3 Preliminaries and Problem Formulation

Following the formulation introduced in [27], let \mathcal{X} and \mathcal{Y} be the input (images) and output (label) spaces, respectively, and $\mathcal{D} = \{(x_i, y_i)\}_{i=1}^N$ be a training dataset of N samples drawn from $\mathcal{X} \times \mathcal{Y}$. We are interested in learning a classification model $f_\theta : \mathcal{X} \rightarrow \mathcal{Y}$, parameterized by $\theta \in \Theta$, by minimizing the average loss (e.g. cross-entropy) across training samples *i.e.* $\frac{1}{N} \sum_{i=1}^N \ell(f_\theta(x_i), y_i)$. We work under the hypothesis that, due to the presence of spurious correlations, the model could incur in biased predictions, failing to generalize at test time. To formulate the spurious correlations, let $\mathcal{A} = \{a_1, \dots, a_n\}$ denote a set of spurious attributes, where $a_i(x) \in \{0, 1\}$ indicates that the attribute a_i is present in the image x . In the presence of spurious correlation between an attribute a_i and a target label y , the model learns to rely on it rather than the real target features to make predictions. This results in the model performing poorly on examples of class y that do not contain the spurious feature a_i .

The dataset \mathcal{D} is partitioned into different and not equally distributed groups or slices. A group is defined based on the combination of the target labels $y \in \mathcal{Y}$ and the spurious attributes $a_i \in \mathcal{A}$ that spuriously correlates with the label (*i.e.* $\mathcal{G} = \mathcal{A} \times \mathcal{Y}$). Formally, given a pair (a_i, y^*) , we define a group or slice $g(a_i, y^*)$ as the set of data samples labeled with y^* which contain attribute a_i , *i.e.* where $a_i(x) = 1$.

For example, in the CelebA dataset [17], where the task involves classifying people with blond hair, the spurious attribute is the person’s gender, as there is a higher frequency of blond women in the dataset. Figure 1 illustrates this issue for the CelebA dataset, and a similar case found in the Waterbirds dataset [20], highlighting the classes with the least training samples per group. The groups with the largest number of samples are where the correlations hold, whereas the

groups with the smallest number of samples are where the correlations do not hold.

Training a model by simply minimizing the average error can lead to rely on spurious features, like gender to predict hair color in the CelebA dataset. Consequently, the model may perform poorly on minority groups where this spurious correlation does not hold. Following [27], we consider a function $M : \mathcal{A} \rightarrow \mathcal{Y}$ that maps each spurious attribute to the unique label that is most associated with it. Then, the unsupervised bias discovery problem is defined as finding the groups (or slices) G , where attribute a_i is spuriously correlated with label y as:

$$G = \left\{ g(a_i, y) \mid \forall a, y \in \mathcal{A} \times \mathcal{Y}, M(a) = y \right\} \quad (1)$$

4 ViG-Bias: Visually Grounded Bias Discovery and Mitigation

In this section, we present the proposed method for discovering biases using visual explanations. We first provide quantitative evidence showing that visual explanations tend to correlate with spurious features, and then propose using them to drive the attention and improve performance for a variety of bias discovery and mitigation methods.

Consider a dataset D with samples $(x, y, a) \in \mathcal{D}$ drawn from $\mathcal{X} \times \mathcal{Y} \times \mathcal{A}$, where a is spuriously correlated with the label y . We are interested in discovering the visual features upon which a model have relied to make a prediction. Prior work [11,22] suggests that, under the presence of spurious correlations, visual explanations for models trained with standard empirical risk minimization (ERM) tend to focus on such shortcuts, while ignoring the core features. We thus resort to GradCAM heatmaps generated using an image classifier that was trained with standard ERM on the dataset of interest \mathcal{D} . Such heatmaps will then be used as visual explanations to guide the attention of bias discovery methods (alternative visual explanation methods like ScoreCAM [26], FullGrad [23], GradCAM++ [4] are also evaluated in Section 6.3). GradCAM heatmaps are obtained by first computing the gradients of the target class with respect to the feature maps of the last convolutional layer, as neurons in this layer offer best compromise between high-level semantics and detailed spatial information [21]. These gradients flowing back are then globally-averaged over the width and height dimensions to obtain the importance weights of every feature map in this last layer. Then, the ReLU activation function is applied on the weighted average of the feature maps, so that only the features that have a positive influence on the class of interest are finally highlighted. These heatmaps are finally normalized between 0 and 1.

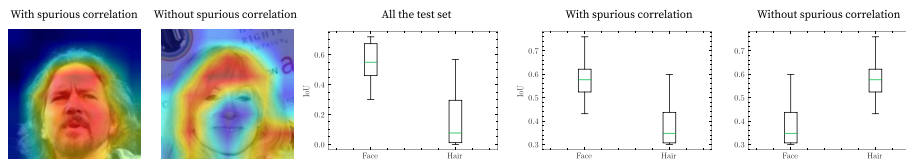


Fig. 2: Visual explanation methods (e.g. GradCAM [21] for the class *blond*) help with identifying spurious correlations. We use the Intersection-over-Union (IoU) metric to measure the percentage of overlap between a binary image representing the spurious feature and the image we get after applying a visual explanation methods.

4.1 Are Visual Explanations Focusing on Spurious Correlations?

The work of Krishnakumar [14] and colleagues provides qualitative examples showing that GradCAM heatmaps for biased models tend to focus on spurious correlations. Here we perform a more systematic quantitative evaluation to confirm this hypothesis. To this end, we design a simple experiment using the CelebA (where the conflicting slices are well known) that consists of three steps:

1. We first construct binary segmentation masks m_i^c and m_i^s for all images x_i in both datasets, segmenting the core features associated to the object of interests (m_i^c representing *hair* in CelebA), and the spurious attribute (m_i^s representing the *face*) as shown in Figure 1. We do so by using LangSAM³, an open-source model that combines Segment Anything Model (SAM) [13] with GroundingDINO [16] to enable instance segmentation from text prompts.
2. We then proceed to create binary masks b_i by thresholding the heatmaps obtained via GradCAM as $b_i = \text{GradCAM}(x_i) \geq \tau$. These masks represent the area where the biased model focuses its attention (we use $\tau = 0.7$ in our experiment which was chosen by visual inspection).
3. Finally, we measure the intersection over union (IoU) between the GradCAM masks b_i , and both, the core (m_i^c) and spurious (m_i^s) segmentations.

Figure 2 shows the results of this motivational experiment. As it can be observed, GradCAM masks coming from bias-conflicted cases (with spurious correlations) tend to present a significantly higher overlap with the spurious features, what in this case implies focusing directly on the face instead of the hair. With this quantitative experiment confirming our initial hypothesis, we proceed to describe the ViG-Bias framework, showing how visual explanations can be easily integrated to improve performance in a variety of existing bias discovery and mitigation methods.

4.2 Improving Unsupervised Bias Discovery via Visual Explanations

ViG-Bias is based on a simple yet effective idea: use visual explanations to direct the attention of bias discovery methods towards real spurious features. Let us

³ <https://github.com/luca-medeiros/lang-segment-anything>

define a mapping function $h : \mathcal{X} \rightarrow \mathcal{X}$, that is applied to an input image x to highlight areas where a given classifier is focusing, as:

$$h(x) = \mathbb{1}\{x \odot \text{GradCAM}(x) \geq \tau\} \quad (2)$$

where \odot represents the Hadamard (element-wise) product of the input image x and the heatmap produced by the GradCAM (or other visual explanation method). We argue that such simple function can help to improve the performance of recent bias discovery methods based on cross-modal feature clustering (e.g. DOMINO [7] and FACTS [27]) and image captioning (e.g. Bias-to-text [12]). In the following sections, we discuss how visual explanations can be incorporated into each of the aforementioned methods.

Visually Grounded DOMINO (ViG-DOMINO): DOMINO uses cross-modal embeddings to identify coherent conflicting slices and generate natural language descriptions to describe them. To this end, they first project the images into a cross-modal embedding (e.g. CLIP [19]). Then, given a classifier that was trained using a standard ERM procedure, predictions for each image are obtained. These predictions are then combined with the cross-modal embeddings and the true labels associated with the input image. An error-aware mixture model is finally fit to cluster slices that are homogeneous not only semantically, but also with respect to error type (e.g. all false positives). Finally, natural language descriptions of the discovered slices are produced to describe characteristics shared between examples in the discovered slices. For more details about DOMINO please refer to [7].

We modify DOMINO by simply pre-processing the images before the cross-modal embeddings are obtained, i.e. we generate heatmaps using the pretrained classifier and extract embeddings for $h(x)$ instead of x . Note that other type of visual explanation methods could also be used, as discussed in Section 6.3.

Visually Grounded FACTS (ViG-FACTS): The FACTS method is similar to DOMINO, but it consists of a two-stage process, where biases are first amplified and then slicing is performed. In the first stage, we increase the model’s reliance on spurious, often bias-indicative correlations, which are amplified using regularization. In general, regularization helps in preventing overfitting and encourage the model to learn more robust patterns that are assumed to be applicable beyond the training set. However, in FACTS, the regularization is applied to constrain the model’s capacity and learn the bias-aligned slices where spurious correlation holds. This leads to the model developing a strong dependency on these correlations, making the biases more pronounced and identifiable. Once these biases are amplified and more clearly delineated, the second stage of the process, *slicing*, an error-aware mixture model that uses the CLIP embeddings similarly to DOMINO is applied.

We modify FACTS the same way as we modified DOMINO, by applying the mapping $h(x)$ to the input images before embedding them to CLIP.

Visually Grounded Bias-to-Text (ViG-B2T): In contrast to the methods described above that focus on discovering conflicting slices on the cross-modal embeddings, B2T first generates textual image descriptions which are then pro-

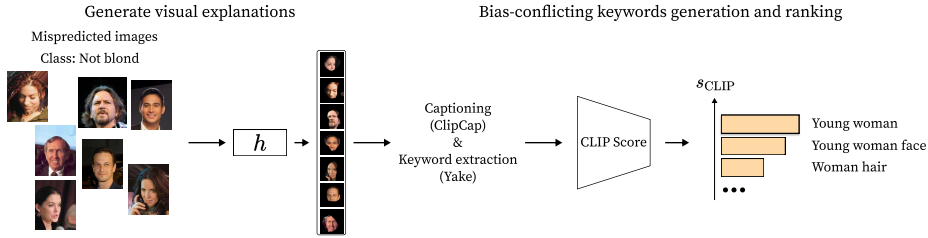


Fig. 3: The B2T framework treats visual biases as language, allowing to (1) uncover new biases by interpreting keywords and (2) mitigate biases in models by leveraging these identified keywords. Through B2T, spurious correlations between attributes like *female* and *blond* are uncovered. To enhance this process, we suggest integrating a visual explanation component before keyword generation. This addition aims to improve the relevance of identified keywords and assess the effectiveness of using these keywords in debiasing.

cessed to identify the conflicting slices. The ClipCap [18] image captioning model is used to generate textual descriptions. Then, keywords are extracted for the incorrectly predicted samples, and ranked using the CLIP score to determine which ones are related to the spurious attributes, based on their similarity with correctly or incorrectly classified images. Formally, the CLIP score is given by:

$$s_{\text{CLIP}}(k, \mathcal{D}) = \text{sim}(k, \mathcal{D}_{\text{wrong}}) - \text{sim}(k, \mathcal{D}_{\text{correct}}) \quad (3)$$

where $\mathcal{D}_{\text{wrong}}$ and $\mathcal{D}_{\text{correct}}$ are the set of correctly and incorrectly classified images, respectively, and $\text{sim}(a, \mathcal{D})$ is the similarity between the keyword k and the dataset \mathcal{D} . Keywords with the highest CLIP score are considered to describe the spurious attributes. Figure 3 illustrates the overall framework of B2T method.

We modify B2T and improve the quality of the bias description keywords by focusing the attention of the image captioning model into the spurious features using visual explanations. Therefore, before generating the captions, we first apply function $h(x)$ to the images, then generate the captions, extract the keywords and rank them as originally proposed in [12]. Figure 3 illustrates the B2T method, and how we utilize visual explanations.

4.3 Improving bias mitigation via visual explanations

Although the methods described above are effective in discovering biases in image classifiers, they do not provide a direct way to mitigate them. In this section, we describe how bias mitigation methods can benefit from visual explanations to improve worst-group accuracy. Here we focus on two alternatives: using language-based zero-shot classifiers, and Group Distributionally Robust Optimization (GroupDRO) [20].

Zero-shot Classifier. Language-based Zero-shot (ZS) classification can be defined as the task of predicting a class that has not been explicitly seen during training, by leveraging the semantic understanding encoded in its pre-trained

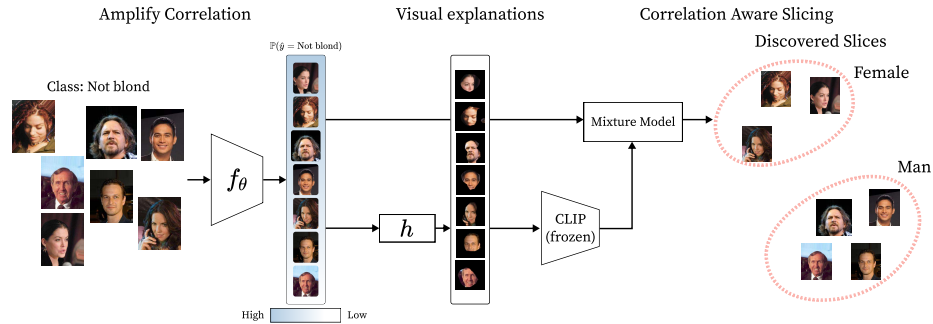


Fig. 4: Our objective is to pinpoint slices of data where a spurious correlation exists between a task-irrelevant attribute (such as gender) and the task label of interest. For instance, in the given example, above, this corresponds to not blond in male or female, while not blond male forms a bias-aligned slice. FACTS amplifies correlations, aiming to establish a straightforward bias-aligned hypothesis. Then, it applies a visual explanation to the dataset using the amplified model. Finally, correlation-aware slicing is executed, a process in which clustering is conducted within the bias-amplified feature space. To enhance this process, we suggest integrating a visual explanation component h before keyword generation.

embeddings (*e.g.*, using cross-modal embeddings like CLIP [19]). Prior studies proposed several prompting strategies to mitigate biases in ZS classifiers. [28] employs group-informed prompting, which performs zero-shot classification using prompts with group information (*e.g.*, “a waterbird on a land background”), what has shown to reduce the gap between worst and average-class accuracy. Since this approach still requires having access to the group names, which is not the case in our setting, we follow [12] and employ a prompting strategy that mitigates biases in ZS classifiers by augmenting the base prompt with conflicting keywords discovered by B2T and our visually grounded variant, ViG-B2T. Importantly, we show that the words discovered by ViG-B2T actually lead to improved mitigation performance.

Group Distributionally Robust Optimization (GroupDRO). As discussed in the Section 2, GroupDRO [20] is effective at mitigating biases but it requires pre-defined group annotations. Formally, for some loss functions ℓ (*e.g.* cross-entropy) and training data $\{(x_i, y_i, g_i)\}_{i=1}^N$ with N samples, the GroupDRO objective is given by:

$$\min_{\theta \in \Theta} \left\{ \max_{g \in \mathcal{G}} \frac{1}{n_g} \sum_{i=1|g_i=g}^{n_g} \ell(f_\theta(x_i), y_i) \right\} \quad (4)$$

where n_g is the number of samples per group. The original B2T proposes inferring group annotations using the language-based zero-shot classifier, CLIP [19], and then re-train a classifier using the GroupDRO algorithm with the new group annotations. Here we evaluate the performance of GroupDRO when trained using the keywords inferred by the original B2T and our proposed ViG-B2T.

5 Experiments

We study three datasets: CelebA [17], Waterbirds [20] and NICO++ [29], which are standard benchmarks for evaluating the discovery and mitigation of biases caused by spurious correlations. All the details about the datasets can be found in Supplementary Material A. Moreover, all implementation details of our method are presented in Supplementary Material B.

5.1 Evaluation Protocol

Bias Discovery Metrics. In our study, we adopt the `Precision@k` metric [7] to assess the effectiveness of our slice discovery methodology in identifying bias-conflicting slices within a dataset. This metric measures the proportion of the top k elements in the discovered slice that are in the ground-truth slice. For more details we refer to [7].

Bias Mitigation Metrics. To evaluate the bias mitigation performance, we use two different metrics: average and worst-case accuracy. Following [20], we report an adjusted average accuracy, which is the test accuracy across all groups, weighted by the number of samples in each group in the training data. The worst-group accuracy (WGA) is the lowest accuracy across all groups defined as, $\min_{g \in \mathcal{G}} \frac{1}{n_g} \sum_{i=1}^{n_g} \mathbb{1}\{f_{\theta}(x) = y\}$ where n_g is the number of samples per group.

5.2 Comparison Baselines

Bias Discovery Baselines. Our objective is to assess the impact of incorporating visual explanations into a bias discovery method and determine whether it enhances the effectiveness of the bias discovery process. Thus, the baseline methods consist of the standard versions of the bias discovery methods, for this comparison we include B2T [12], FACTS [27], and DOMINO [7].

Bias Mitigation Baselines. Regarding debiasing methods, our aim is to assess the influence of visual explanations on their formulation. As outlined in Section 4.3, our approach involves extracting keywords associated with spurious attributes and informed using visual explanations, forming groups through zero-shot classification based on these keywords and labels, and subsequently training a GroupDRO [20] model based on the generated groups. We intend to compare these methods with the standard versions which do not incorporate visual explanations. Additionally, we will compare them with a standard version of GroupDRO [20] where groups are built using the ground-truth attributes already present in the dataset, as well as with another mitigation method, JTT [15], which does not rely on group information.

6 Results

6.1 Evaluating Bias Discovery

We first evaluate the quality of the predicted slices with and without utilizing visual explanations in Table 1. As in [27], we use the metric `Precision@k`, and we

Table 1: Visual explanations enhance the effectiveness of bias discovery methods. We report $precision@k$ as a metric to assess the quality of slices generated by each method.

Method	Datasets				
	Waterbirds	CelebA	NICO++ ⁷⁵	NICO++ ⁹⁰	NICO++ ⁹⁵
DOMINO [7]	90.0%	87.0%	24.0%	24.0%	24.0%
ViG-DOMINO (ours)	92.0%	90.0%	25.0%	24.0%	25.4%
B2T [12]	92.0%	64.0%	-	-	-
ViG-B2T (ours)	97.0%	70.0%	-	-	-
FACTS [27]	100.0%	100.0%	55.0%	60.8%	61.0%
ViG-FACTS (ours)	100.0%	100.0%	60.0%	66.7%	65.0%

set $k = 10$. Unlike DOMINO and FACTS, B2T does not assume that each target label may be mapped to multiple spurious features. Moreover, the discovered keywords in B2T reflect only the dominant spurious feature per class. That is why we could not report its results on the NICO++ dataset (note that the original B2T publication does not report results on NICO++ neither). Nonetheless, the accuracy of the inferred slices when using visual explanations in B2T on Waterbirds and CelebA datasets shows systematic improvement. Importantly, incorporating visual explanations into bias discovery methods yields either the same or better $Precision@k$ across all five datasets.

6.2 Evaluating Bias Mitigation

We then evaluate the effectiveness of the identified slices and keywords in reducing spurious correlations. Initially, we assess the average and worst-group accuracies for zero-shot classification tasks using various prompting strategies. Then, we compare debiasing models using the GroupDRO algorithm, each using the discovered keywords to infer the new group annotations across all datasets. **Evaluating Zero-Shot Classification.** Results shown in Table 2 reveal that incorporating visual explanations enhances worst group accuracy across all datasets and reduces the gap between worst and average accuracy, resulting in significant improvements. For instance, in the Waterbird dataset, we achieve an 8% increase in worst group accuracy compared to Zero-shot classification without visual explanation. Similarly, in CelebA, we observe a 1.2% enhancement in worst group accuracy.

Debiasing Classifiers With GroupDRO. We compare the bias mitigation performance when training a classifier using GroupDRO considering three different group definitions: (1) using the ground-truth attributes (e.g. *male* and *female* for CelebA, or *land* and *water* for Waterbirds), (2) using inferred groups obtained from standard B2T [12] and (3) incorporating visual explanations in the creation of the inferred groups via ViG-B2T. Additionally, we compare our approach with JTT [15], which do not use group information, and standard ERM. Results are presented in Table 3, showing that integrating visual expla-

Table 2: Visual explanations improve the effectiveness of bias mitigation approaches. We report worst group accuracy and average accuracy across all groups (the higher the better) and gap between these two (the lower, the better).

Prompting strategy	Waterbirds			CelebA			NICO++ ⁷⁵			NICO++ ⁹⁰			NICO++ ⁹⁵		
	Worst	Avg.	Gap	Worst	Avg.	Gap	Worst	Avg.	Gap	Worst	Avg.	Gap	Worst	Avg.	Gap
ZS w/ Base prompt [19]	51.0%	79.0%	28%	69.4%	81.9%	12.5%	70.7%	76.0%	5.3%	70.3%	76.6%	6.3%	68.2%	77.3%	9.1%
ZS + Group labels [28]	50.3%	82.7%	32.4%	71.6%	90.2%	18.6%	75.3%	76.8%	1.5%	75.8%	77.2%	1.4%	75.1%	77.7%	2.6%
ZS + B2T Groups [12]	55.0%	76.3%	21.3%	77.5%	86.4%	8.9%	77.0%	77.6%	0.6%	69.9%	75.0%	5.1%	77.1%	75.0%	2.1%
ZS + ViG-B2T Groups (ours)	63.1%	77.8%	14.7%	78.2%	85.2%	7%	77.9%	79.4%	1.5%	75.3%	80.6%	5.3%	74.6%	81.1%	6.5%

Table 3: Incorporating visual explanations improves the effectiveness of bias mitigation approaches, particularly in terms of worst group accuracy, a commonly utilized metric in bias mitigation tasks.

Method	Uses group information	Waterbirds			CelebA		
		Worst	Avg.	Gap	Worst	Avg.	Gap
ERM	No	62.4%	97.7%	35.3%	47.0%	94.9%	47.9%
JTT [15]		86.3%	92.8%	6.5%	82.0%	88.0%	6%
GroupDRO w/ original groups [20]	Yes	88.0%	93.7%	5.7%	88.4%	91.6%	3.2%
GroupDRO w/ B2T groups [12]		88.3%	93.8%	5.5%	87.8%	92.7%	4.9%
GroupDRO w/ ViG-B2T groups (ours)		90.2%	93.4%	3.2%	91.0%	93.9%	2.9%

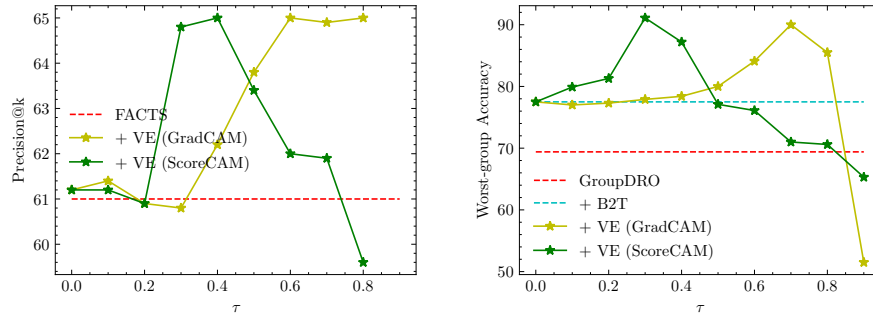
nations enhances worst group accuracy across all datasets, and yields the lowest gap between worst and average accuracy.

6.3 Ablations

We perform ablation studies considering an alternative visual explanation method (ScoreCAM [26], which differently from GradCAM, does not rely on gradients to construct the class activation maps) and different thresholds τ for the generation of the binary masks. Figure 5 shows results both for bias discovery (Figure 5a) and mitigation (Figure 5b). We aim to assess the stability of the visual explanation methods across different threshold levels. We find that both, GradCAM and ScoreCAM achieve approximately similar worst group accuracies for different values of τ . For instance, ScoreCAM gets good worst-group accuracy at lower threshold values, whereas GradCAM [21] requires increasing threshold values. Nevertheless, the worst group accuracy remains approximately constant for both methods. Finally, some qualitative results from these visualizations are provided in Figure 6 for different attention methods. Some more visual results are also included in Supplementary Material C.

7 Conclusion

Bias discovery and mitigation remain critical challenges in the deployment of fair and reliable machine learning models. In this paper, we introduced Visually Grounded Bias Discovery (ViG-Bias), a novel method that leverages visual



(a) We plot the value of the Precision@k obtained after fitting the mixture model in FACTS with and without incorporating visual explanations against the threshold τ , and compare ViG-FACTS (GradCAM) and ViG-FACTS (ScoreCAM) for visual explanation capabilities on the CelebA datasets.

(b) We plot the value of the worst-group accuracy obtained using GroupDRO with ViG-B2T groups classifier, as the threshold τ increases for GroupDRO with ViG-B2T (GradCAM) and GroupDRO with ViG-B2T (ScoreCAM) on the CelebA dataset.

Fig. 5: Ablating the GradCAM [21] mask threshold τ on the CelebA dataset for bias discovery (a) and mitigation (b).

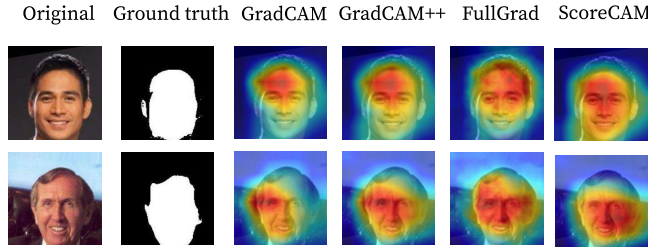


Fig. 6: Visual explanations of other CAM-variants (GradCAM++ [4], Fullgrad [23] and ScoreCAM [26]) for a biased model trained on CelebA. Compared to other CAM methods, ScoreCAM tends to better highlight the region related to the spurious feature (in this case, instead of focusing on the hair, it points to the face), for images from groups where the spurious correlation holds.

explanations to uncover and address biases in visual recognition models. By integrating multimodal embeddings with visual explanation techniques, ViG-Bias not only identifies biases with higher precision but also provides insights into the nature of these biases, facilitating the development of more equitable models.

Our approach represents a significant step forward in unsupervised bias discovery and mitigation research by offering a method that is both effective and interpretable, while easily adaptable to multiple existing frameworks. The systematic improvements observed across various datasets underscore the utility of visual explanations in enhancing model fairness and reliability, by reducing their dependence on spurious correlations.

As future work, we aim to investigate the integration of ViG-Bias with other bias detection and mitigation frameworks to further enhance its effectiveness and adaptability.

8 Acknowledgments

We gratefully acknowledge the DATAIA program for supporting EF as a visiting professor at Université Paris-Saclay, NVIDIA Corporation for providing GPU computing, the support of Agencia Nacional de Promoción de la Investigación, el Desarrollo Tecnológico y la Innovación (Argentina), the Google Award for Inclusion Research (AIR) Program and the SticAmSud program.

References

1. Alicioglu, G., Sun, B.: A survey of visual analytics for explainable artificial intelligence methods. *Computers & Graphics* **102**, 502–520 (2022) [2](#)
2. Barocas, S., Hardt, M., Narayanan, A.: *Fairness and machine learning: Limitations and opportunities*. MIT Press (2023) [2](#)
3. Buolamwini, J., Gebru, T.: Gender shades: Intersectional accuracy disparities in commercial gender classification. In: *Conference on fairness, accountability and transparency*. pp. 77–91. PMLR (2018) [2](#)
4. Chattopadhyay, A., Sarkar, A., Howlader, P., Balasubramanian, V.N.: Grad-cam++: Generalized gradient-based visual explanations for deep convolutional networks. In: *2018 IEEE Winter Conference on Applications of Computer Vision (WACV)*. IEEE (Mar 2018). <https://doi.org/10.1109/wacv.2018.00097>, <http://dx.doi.org/10.1109/WACV.2018.00097> [6](#), [14](#)
5. Deng, J., Dong, W., Socher, R., Li, L.J., Li, K., Fei-Fei, L.: Imagenet: A large-scale hierarchical image database. In: *2009 IEEE Conference on Computer Vision and Pattern Recognition*. pp. 248–255 (2009). <https://doi.org/10.1109/CVPR.2009.5206848> [17](#)
6. Du, Y., Liu, Z., Li, J., Zhao, W.X.: A survey of vision-language pre-trained models. arXiv preprint arXiv:2202.10936 (2022) [2](#)
7. Eyuboglu, S., Varma, M., Saab, K., Delbrouck, J.B., Lee-Messer, C., Dunnmon, J., Zou, J., Ré, C.: Domino: Discovering systematic errors with cross-modal embeddings (2022) [2](#), [3](#), [8](#), [11](#), [12](#), [17](#)
8. Geirhos, R., Jacobsen, J.H., Michaelis, C., Zemel, R., Brendel, W., Bethge, M., Wichmann, F.A.: Shortcut learning in deep neural networks. *Nature Machine Intelligence* **2**(11), 665–673 (2020) [2](#)
9. Gildenblat, J., contributors: Pytorch library for cam methods. <https://github.com/jacobgil/pytorch-grad-cam> (2021) [18](#)
10. He, K., Zhang, X., Ren, S., Sun, J.: Deep residual learning for image recognition (2015) [17](#)
11. Joshi, S., Yang, Y., Xue, Y., Yang, W., Mirzasoleiman, B.: Towards mitigating spurious correlations in the wild: A benchmark and a more realistic dataset (2023) [6](#)
12. Kim, Y., Mo, S., Kim, M., Lee, K., Lee, J., Shin, J.: Bias-to-text: Debiasing unknown visual biases through language interpretation (2023) [2](#), [3](#), [4](#), [8](#), [9](#), [10](#), [11](#), [12](#), [13](#), [17](#), [18](#)

13. Kirillov, A., Mintun, E., Ravi, N., Mao, H., Rolland, C., Gustafson, L., Xiao, T., Whitehead, S., Berg, A.C., Lo, W.Y., et al.: Segment anything. arXiv preprint arXiv:2304.02643 (2023) [7](#)
14. Krishnakumar, A., Prabhu, V., Sudhakar, S., Hoffman, J.: Udis: Unsupervised discovery of bias in deep visual recognition models. In: British Machine Vision Conference (BMVC). vol. 1, p. 3 (2021) [2](#), [3](#), [7](#)
15. Liu, E.Z., Haghgoo, B., Chen, A.S., Raghunathan, A., Koh, P.W., Sagawa, S., Liang, P., Finn, C.: Just train twice: Improving group robustness without training group information (2021) [4](#), [11](#), [12](#), [13](#)
16. Liu, S., Zeng, Z., Ren, T., Li, F., Zhang, H., Yang, J., Li, C., Yang, J., Su, H., Zhu, J., et al.: Grounding dino: Marrying dino with grounded pre-training for open-set object detection. arXiv preprint arXiv:2303.05499 (2023) [7](#)
17. Liu, Z., Luo, P., Wang, X., Tang, X.: Deep learning face attributes in the wild. In: Proceedings of International Conference on Computer Vision (ICCV) (December 2015) [5](#), [11](#), [17](#)
18. Mokady, R., Hertz, A., Bermano, A.H.: Clipcap: Clip prefix for image captioning (2021) [9](#), [19](#)
19. Radford, A., Kim, J.W., Hallacy, C., Ramesh, A., Goh, G., Agarwal, S., Sastry, G., Askell, A., Mishkin, P., Clark, J., Krueger, G., Sutskever, I.: Learning transferable visual models from natural language supervision (2021) [8](#), [10](#), [13](#), [18](#)
20. Sagawa, S., Koh, P.W., Hashimoto, T.B., Liang, P.: Distributionally robust neural networks for group shifts: On the importance of regularization for worst-case generalization (2020) [4](#), [5](#), [9](#), [10](#), [11](#), [13](#), [17](#), [18](#)
21. Selvaraju, R.R., Cogswell, M., Das, A., Vedantam, R., Parikh, D., Batra, D.: Grad-cam: Visual explanations from deep networks via gradient-based localization. *International Journal of Computer Vision* **128**(2), 336–359 (Oct 2019). <https://doi.org/10.1007/s11263-019-01228-7>, <http://dx.doi.org/10.1007/s11263-019-01228-7> [3](#), [6](#), [7](#), [13](#), [14](#)
22. Singla, S., Feizi, S.: Salient imagenet: How to discover spurious features in deep learning? (2022) [3](#), [6](#)
23. Srinivas, S., Fleuret, F.: Full-gradient representation for neural network visualization (2019) [6](#), [14](#)
24. Sun, S., Koch, L.M., Baumgartner, C.F.: Right for the wrong reason: Can interpretable ml techniques detect spurious correlations? In: International Conference on Medical Image Computing and Computer-Assisted Intervention. pp. 425–434. Springer (2023) [2](#)
25. Wah, C., Branson, S., Welinder, P., Perona, P., Belongie, S.: The caltech-ucsd birds-200-2011 dataset (Aug 2023) [17](#)
26. Wang, H., Wang, Z., Du, M., Yang, F., Zhang, Z., Ding, S., Mardziel, P., Hu, X.: Score-cam: Score-weighted visual explanations for convolutional neural networks (2020) [6](#), [13](#), [14](#)
27. Yenamandra, S., Ramesh, P., Prabhu, V., Hoffman, J.: Facts: First amplify correlations and then slice to discover bias (2023) [3](#), [4](#), [5](#), [6](#), [8](#), [11](#), [12](#), [17](#)
28. Zhang, M., Ré, C.: Contrastive adapters for foundation model group robustness (2022) [10](#), [13](#)
29. Zhang, X., He, Y., Xu, R., Yu, H., Shen, Z., Cui, P.: Nico++: Towards better benchmarking for domain generalization (2022) [11](#), [17](#)
30. Zhou, B., Lapedriza, A., Khosla, A., Oliva, A., Torralba, A.: Places: A 10 million image database for scene recognition. *IEEE Transactions on Pattern Analysis and Machine Intelligence* **40**(6), 1452–1464 (2018). <https://doi.org/10.1109/TPAMI.2017.2723009> [17](#)

A Datasets

We study three datasets: CelebA [17], Waterbirds [20] and NICO++ [29], which are standard benchmarks for evaluating the discovery and mitigation of biases caused by spurious correlations.

CelebA contains images of celebrities, with various attributes such as *gender*, *hair color*, *age*, *facial hair*, *etc.* We focus on classifying images of celebrities as *blond* or *not blond*, where the spurious attribute is the *gender*, as there is a majority of blond female and non-blond male celebrities. Figure 1 from the main manuscript shows examples for CelebA dataset.

Waterbirds is a collection of images of landbirds and waterbirds from the CUB dataset [25], combined with images from Places dataset [30] as background. The task is to classify the images as landbirds or waterbirds, where the spurious attribute is the background. Figure 1 from the main manuscript illustrates the four groups on Waterbirds dataset. The group of landbirds with a land background, and waterbirds with a water background are the largest, on which the spurious correlation holds.

NICO++ This dataset focuses on real-world images depicting various concepts (*e.g.* dog, bike, wheat, *etc.*) that appear in different contexts (*e.g.* grass, water, beach, *etc.*). It is enhanced with context annotations for six specific environments: dim lighting, outdoor, grass, rock, autumn, and water. These annotations are utilized to create training, validation, and testing splits to facilitate experiments under controlled correlation settings for a 6-way classification task. The variants of the NICO++ dataset, namely NICO++⁹⁵, NICO++⁹⁰, and NICO++⁷⁵, represent different experimental settings that demonstrate how the degree of spurious correlation between the context and the concept affects model performance. The numbers (95, 90, 75) indicate the strength of the correlation β between each concept and its context, as was formulated in [27]. For instance, NICO++⁹⁵ has a stronger correlation between the concept and its context compared to NICO++⁷⁵. Table 4 shows the number of samples for different combinations of context (rows) and target labels (columns), defining slices with spurious correlations in the training split.

B Implementation Details

Following [7], the image classification model is, in all our experiments, a ResNet50 [10] trained using SGD optimizer with a momentum of 0.9, a learning rate of 10^{-5} , a weight decay of 10^{-4} , and a batch size of 64. We start training from ImageNet [5] pre-trained weights for 50 epochs for CelebA, 300 epochs for Waterbirds and 25k steps for NICO++. We use no data augmentation, and no learning rate scheduler.

For all experiments, we use the following implementations: B2T released by [12], FACTS released by [27], and DOMINO released by [7] which were modified

Table 4: Number of samples for different combinations of context (rows) and target labels (columns), defining slices with spurious correlations in the training split.

	mammals	birds	plants	airways	waterways	landways
rock	2552	50	50	50	50	50
grass	24	1280	24	24	24	24
dim lighting	12	12	616	12	12	12
outdoor	16	16	16	879	16	16
water	20	20	20	20	1063	20
autumn	21	21	21	21	21	1104

to incorporate utilize visual explanations. We use the GroupDRO and ERM implementations released by [20], and the library `grad-cam` [9], with state-of-the-art methods for visual explainability.

For B2T experiments, we use pre-trained CLIP models [19] as feature extractors, and, for all datasets, we use the image encoder: ResNet50. For the bias mitigation experiments, we train from scratch all algorithms (ERM, JTT, GroupDRO). In all cases, we report the average and worst-group test accuracies at the epoch with the best validation worst-group accuracy. For the compared methods, we directly use the hyperparameters reported in [12]. For our method, the only hyperparameter we tune is the threshold τ for the heatmap. In general, we observe that as long as the threshold is greater or equal to 0.65, the performance is stable.

C Additional qualitative visualizations and results

C.1 Discovered Keywords by ViG-B2T

Figures 7 and 8 present samples from the CelebA dataset along with the extracted captions, with and without incorporating visual explanations. Note that visually grounded captions tend to mention bias-conflicting keywords more often per class (*man*, *female*, etc.), whereas using a captioning model alone fails to mention those keywords.









Extracted keyword with ViG-B2T	man				woman			
Samples								
Ground truth	not blond	blond	blond	blond	not blond	not blond	blond	not blond
Prediction	not blond	not blond	not blond	not blond	not blond	not blond	not blond	not blond
Caption	person was a member of the hockey team.	actor is the new face of the brand.	actor at the premiere of comedy.	actor - i love the hair on this one.	person, who is a singer, has been performing.	actor with a bob hairstyle.	i want my hair like this!	the beauty of the face.
ViG Caption	a man's face with a red tint.	a man in a suit and tie.	a man with a beard and glasses smiles and looks at the camera.	a man with a white background.	a woman singing into a microphone.	a woman's face with a big smile.	a woman with a white face.	young woman looking at the camera with a serious expression.

Fig. 7: Additional qualitative results from the CelebA dataset, both with (*ViG Caption*) and without (*Caption*) utilizing visual explanations during the process of extracting captions using ClipCap [18]. Visually grounded captions tend to mention bias-conflicting keywords (related to gender in this case) more often.








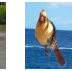
Extracted keyword with ViG-B2T	forest				ocean			
Samples								
Ground truth	waterbird	waterbird	waterbird	landbird	landbird	landbird	landbird	landbird
Prediction	waterbird	landbird	landbird	waterbird	waterbird	waterbird	waterbird	landbird
Caption	biological species, a rare bird.	biological species on the rocks.	biological species in the fall.	a bird in the sky.	a girl flying a kite in the lake.	a surfer gets barreled on a wave.	a bird with a fish.	a bird in flight, with a fish in its beak.
ViG Caption	a static shot of trees and grass in a forest.	a forest of trees grows in the mountains.	a landscape of autumn trees in a forest.	silhouette of a tree against the sky.	a bird in flight over the ocean, clouds in the background.	a man jumps into the ocean.	a bird over the ocean.	biological species flying over the ocean.

Fig. 8: Additional qualitative results from the Waterbirds dataset are provided, both with (*ViG Caption*) and without (*Caption*) utilizing visual explanations during the process of extracting captions using ClipCap. Visually grounded captions tend to mention bias-conflicting keywords (related to the background in this case) more often. [18].

C.2 Complete Tables of Keywords

Tables 5-8 present a comparison between the keywords extracted by B2T and ViG-B2T. We can observe that ViG-B2T extracted keywords which are more relevant to the problem as they are related to spurious correlations, effectively highlighting biases in the dataset. Specifically, ViG-B2T extracted keywords which are related to gender (*male* or *female*), whereas B2T’s keywords only mention *person* without specifying gender, which is crucial information for bias discovery in this case.

Table 5: Top-20 discovered keywords for the *blond* class on the CelebA dataset. Note that B2T method is incapable of extracting keywords that are related to the spurious attribute *gender*, whereas using visual explanations help with extracting the bias-conflicting keywords: *blond males*. We highlight in cyan the more significant keywords discovered using visual explanations, when compared with the standard method.

(a) Using B2T method.			(b) Using ViG-B2T method.		
Keyword	Score	Accuracy	Keyword	Score	Accuracy
player	0.33	0.31	man	1.14	0.95
artist	0.13	0.78	man face	0.94	0.80
film	0.13	0.90	beard	0.64	0.88
actor	0.11	0.88	young	0.23	0.75
person	0.09	0.80	distorted	0.09	0.97
comedy	0.09	0.91	distorted face	0.02	0.82
love	-0.02	0.88	face	-0.02	0.66
face	-0.02	0.84	camera	-0.03	0.85
hair	-0.05	0.89	hair	-0.05	0.92
face of person	-0.08	0.87	big	-0.06	0.96
actor attends	-0.09	0.90	face is distorted	-0.16	0.96
comedy film	-0.11	0.92	face is highlighted	-0.31	0.63
romantic comedy	-0.11	0.91	smiles	-0.38	0.96
actor arrives	-0.14	0.93	smile	-0.39	0.95
contestant	-0.14	0.82	big smile	-0.44	0.98
model	-0.19	0.86	woman hair	-0.8	0.90
romantic comedy film	-0.25	0.91	woman	-0.84	0.86
premiere	-0.52	0.92	woman face	-0.91	0.68
premiere of romantic	-0.69	0.91	young woman	-1.05	0.86
actress	-1.28	0.87	young woman face	-1.2	0.70

Table 6: Top-20 discovered keywords for the *not blond* class on the CelebA dataset.

(a) Using E2T method.			(b) Using ViG-B2T method.		
Keyword	Score	Accuracy	Keyword	Score	Accuracy
actress	2.16	0.97	young woman	2.55	0.98
model	0.56	0.97	young woman face	2.52	0.76
premiere of romantic	0.5	0.97	woman hair	2.05	0.88
hairstyle	0.47	0.89	woman	1.97	0.97
hair	0.39	0.96	woman face	1.81	0.79
premiere	0.2	0.98	woman mouth	1.58	0.67
premiere of comedy	0.11	0.95	hair	0.39	0.94
face of person	0.05	0.96	distorted face	0.28	0.98
romantic comedy film	0.03	0.97	big smile	0.27	0.99
film	0.03	0.98	smile	0.25	0.99
face	0	0.96	distorted	0.23	0.98
romantic comedy	0	0.97	premiere	0.2	0.56
arrives	0	0.97	face is distorted	0.14	0.97
comedy film	-0.09	0.96	face of person	0.05	0.43
person	-0.2	0.98	face	0	0.98
comedy	-0.22	0.96	camera	-0.13	0.98
artist	-0.28	0.96	person	-0.2	0.85
romantic	-0.31	0.97	actor	-0.95	0.09
actor arrives	-0.45	0.97	man face	-1.97	0.50
actor	-0.95	0.97	man	-2.13	0.99

Table 7: Top-20 discovered keywords for the *landbirds* class on the Waterbirds dataset.

(a) Using E2T method.			(b) Using ViG-B2T method.		
Keyword	Score	Accuracy	Keyword	Score	Accuracy
ocean	3.31	0.56	beach	2.64	0.55
beach	2.64	0.74	water	1.31	0.54
seagull	2.55	0.50	sky	0.53	0.84
water	1.31	0.64	rock	0.5	0.67
sunset	1.09	0.69	flight	0.31	0.86
fish	0.97	0.69	white background	0.2	0.81
paradise	0.53	0.90	biological species flying	0.17	0.85
city	0.36	0.69	flying	-0.06	0.88
dog	0.27	0.43	species flying	-0.13	0.85
biological species flying	0.17	0.68	person	-0.13	0.58
person	-0.13	0.8	white	-0.16	0.79
flies	-0.28	0.55	background	-0.17	0.87
biological species	-0.31	0.94	biological species	-0.31	0.91
biological	-0.39	0.94	biological	-0.39	0.91
bird flies	-0.58	0.75	bird flying	-0.5	0.87
species	-0.7	0.94	pond	-0.53	0.44
birds	-1	0.88	species in flight	-0.61	0.80
parrot	-1.03	0.75	species	-0.7	0.91
bird	-1.55	0.93	bird	-1.55	0.93
bird of paradise	-1.69	0.90	biological species perching	-1.67	0.75

Table 8: Top-20 discovered keywords for the *waterbirds* class on the Waterbirds dataset.

(a) Using B2T method.			(b) Using ViG-B2T method.		
Keyword	Score	Accuracy	Keyword	Score	Accuracy
bamboo forest	4.17	0.90	green forest	2.31	0.33
bamboo	3.16	0.68	forest	2.25	0.74
forest	2.25	0.69	trees grows	1.97	0.70
rainforest	2.05	0.33	trees	1.77	0.67
woods	2.02	0.50	tree branch	1.69	0.44
trees	1.77	0.33	large tree	1.56	0.50
tree	1.56	0.59	tree	1.56	0.71
garden	1.52	0.70	branch	1.28	0.40
bird of paradise	1.5	0.50	grass	0.67	0.55
trail	0.5	0.33	green	0.5	0.46
wild	0.16	0.82	flying	-0.08	0.50
prey	0.05	0.84	biological species	-0.16	0.90
bird of prey	0.03	0.84	species	-0.19	0.90
biological species	-0.16	0.75	background	-0.23	0.53
species	-0.19	0.75	bird	-0.25	0.63
bird	-0.25	0.71	bird flying	-0.38	0.43
species of bird	-0.25	0.50	biological	-0.42	0.90
paradise	-0.28	0.50	sky	-0.47	0.55
biological	-0.42	0.75	man	-0.67	0.36
person	-0.63	0.65	close	-0.7	0.6

C.3 Comparing biased and de-biased models using GradCAM

In Figures 9 and 10, we provide a visual comparison of the GradCAM heatmap generated for the classification model, before and after debiasing via GroupDRO and the proposed ViG-GroupDRO. It can be observed that ViG-GroupDRO directs the model focus towards the hair area, which is more informative than the face for the CelebA prediction task (*blond, not blond*). ViG-GroupDRO effectively highlights the hair regions better than GroupDRO.

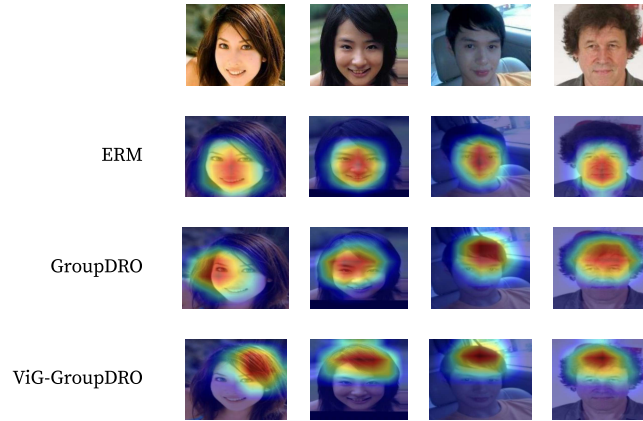


Fig. 9: Visual comparison of the GradCAM Heatmap across ERM, GroupDRO, and ViG-GroupDRO on the CelebA dataset.

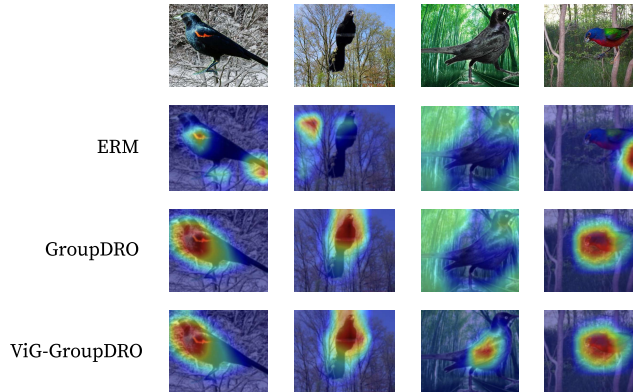


Fig. 10: Visual comparison of the GradCAM Heatmap across ERM, GroupDRO, and ViG-GroupDRO on the Waterbirds dataset.

C.4 Slices discovered by ViG-FACTS

Here we provide some qualitative visualizations showing images which were assigned to different slices by the FACTS algorithm. We show the top-10 images as defined by the likelihood of belonging to the given slice, assigned by the clustering model within FACTS. Note that images in slices for which the mean accuracy is low, tend to correspond to conflicting examples like blond male (Figure 11), non-blond female (Figure 12), water background with land-birds (Figure 13), land background with water-birds (Figure 14), etc.



Fig. 11: Top-10 discovered images per slice for the *blond* class from CelebA dataset.

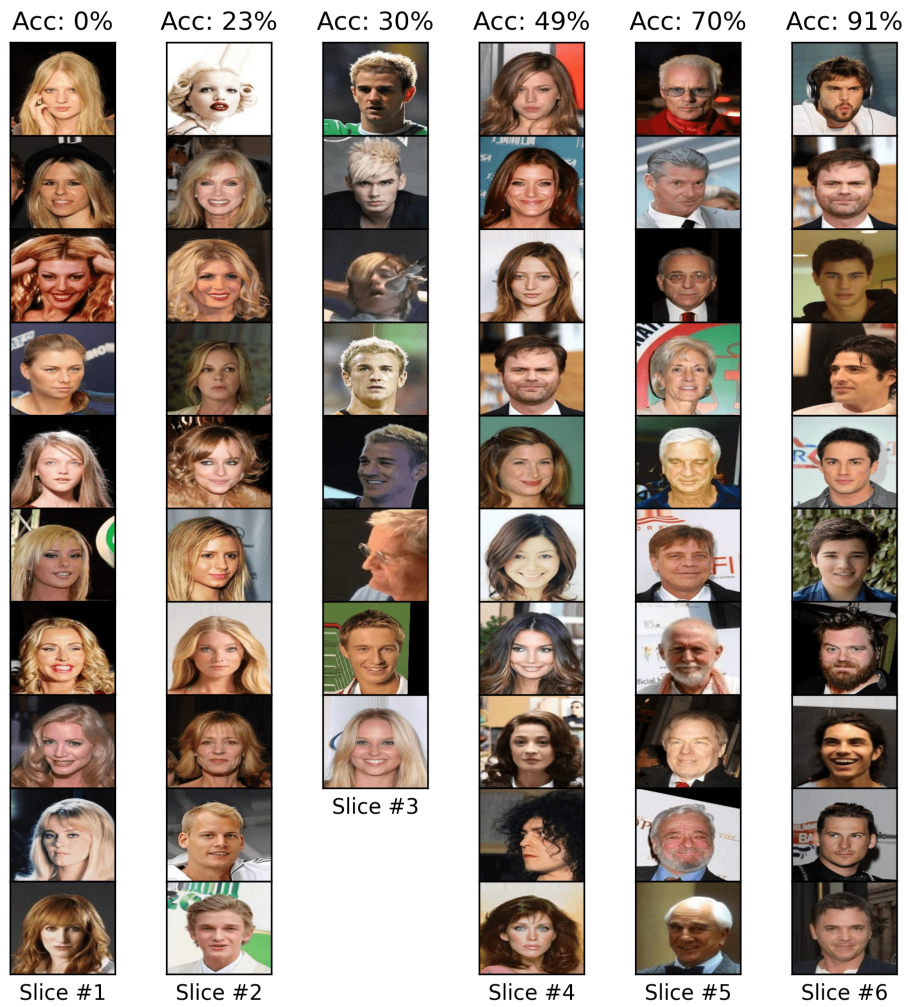


Fig. 12: Top-10 discovered images per slice for the *not blond* class from CelebA dataset.

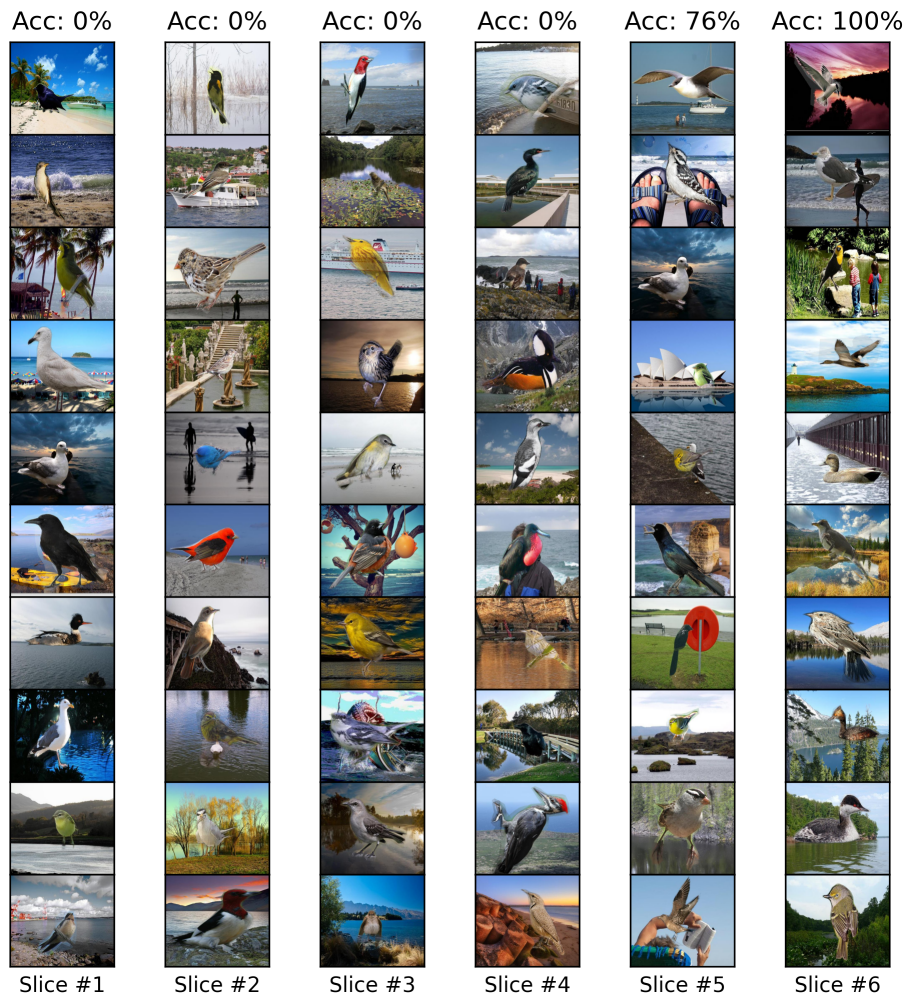


Fig. 13: Top-10 discovered images per slice for the *landbirds* class from Waterbirds dataset. Note that all the extracted slices contain the bias-conflicting slices: land-birds over *water* background.

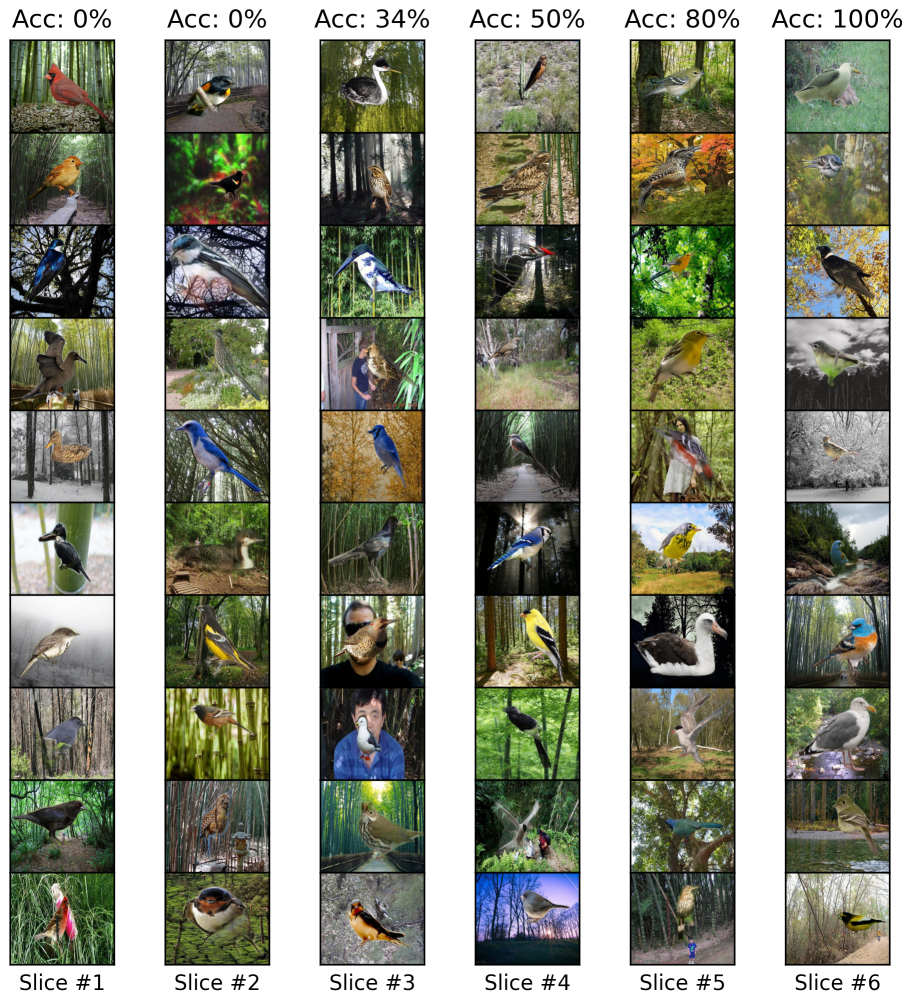


Fig. 14: Top-10 discovered images per slice for the *waterbirds* class from Waterbirds dataset. Note that all the extracted slices contain the bias-conflicting slices: water-birds over *land* background.

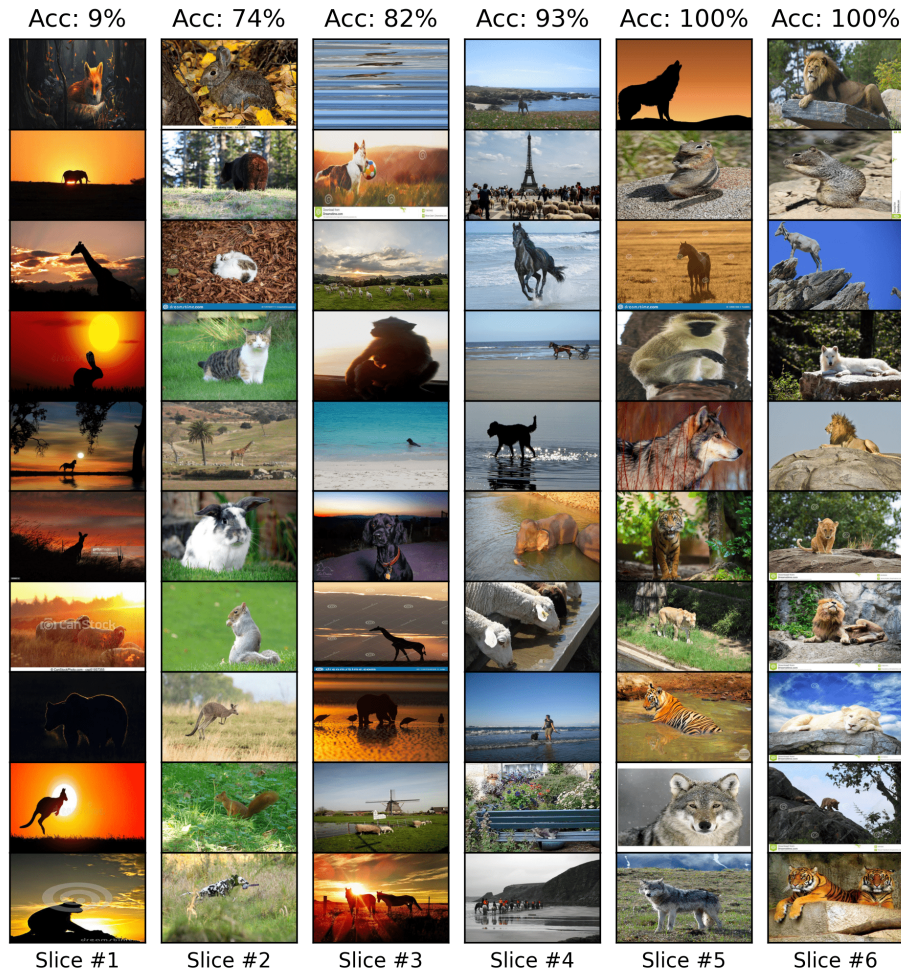


Fig. 15: Top-10 discovered images per slice for the *mammals* class from NICO++⁹⁰ dataset. Note that the last slice corresponds to the slice: *rock*, which is the dominant context (Context with largest number of samples for the *mammals* class in Table 4).

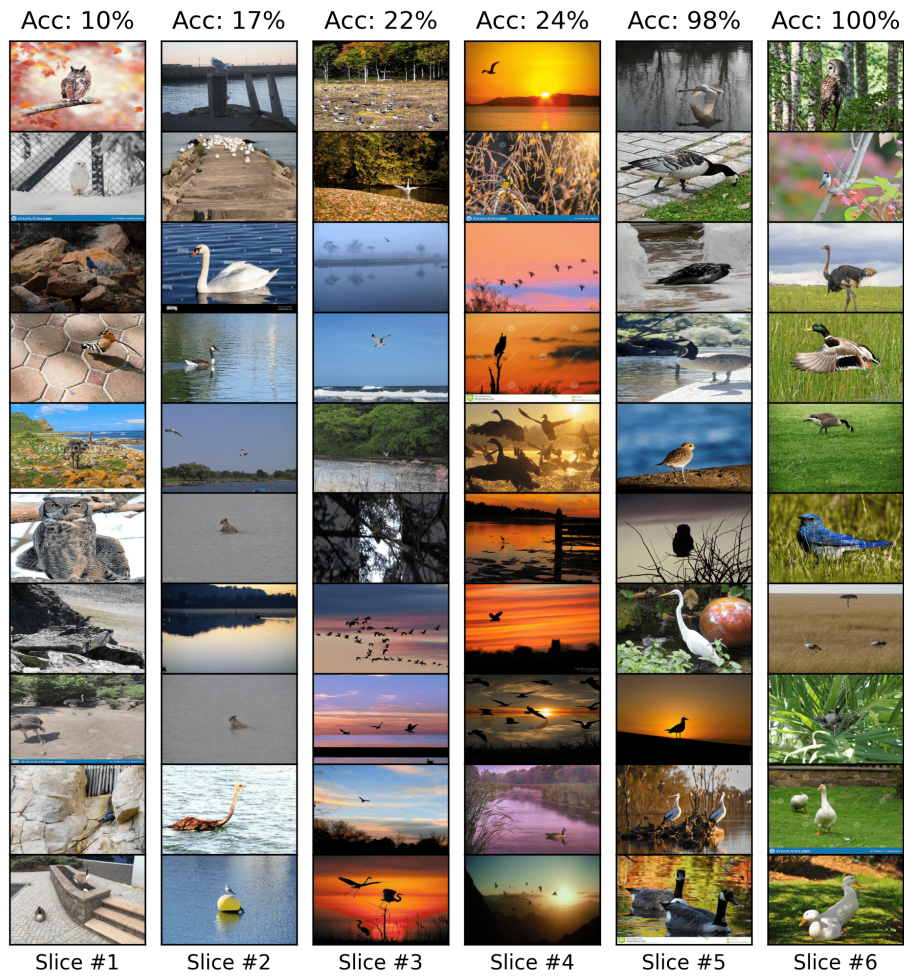


Fig. 16: Top-10 discovered images per slice for the *birds* class from NICO++⁹⁰ dataset. Note that the last slice corresponds to the slice: *grass*, which is the dominant context (Context with largest number of samples for the *grass* class in Table 4).

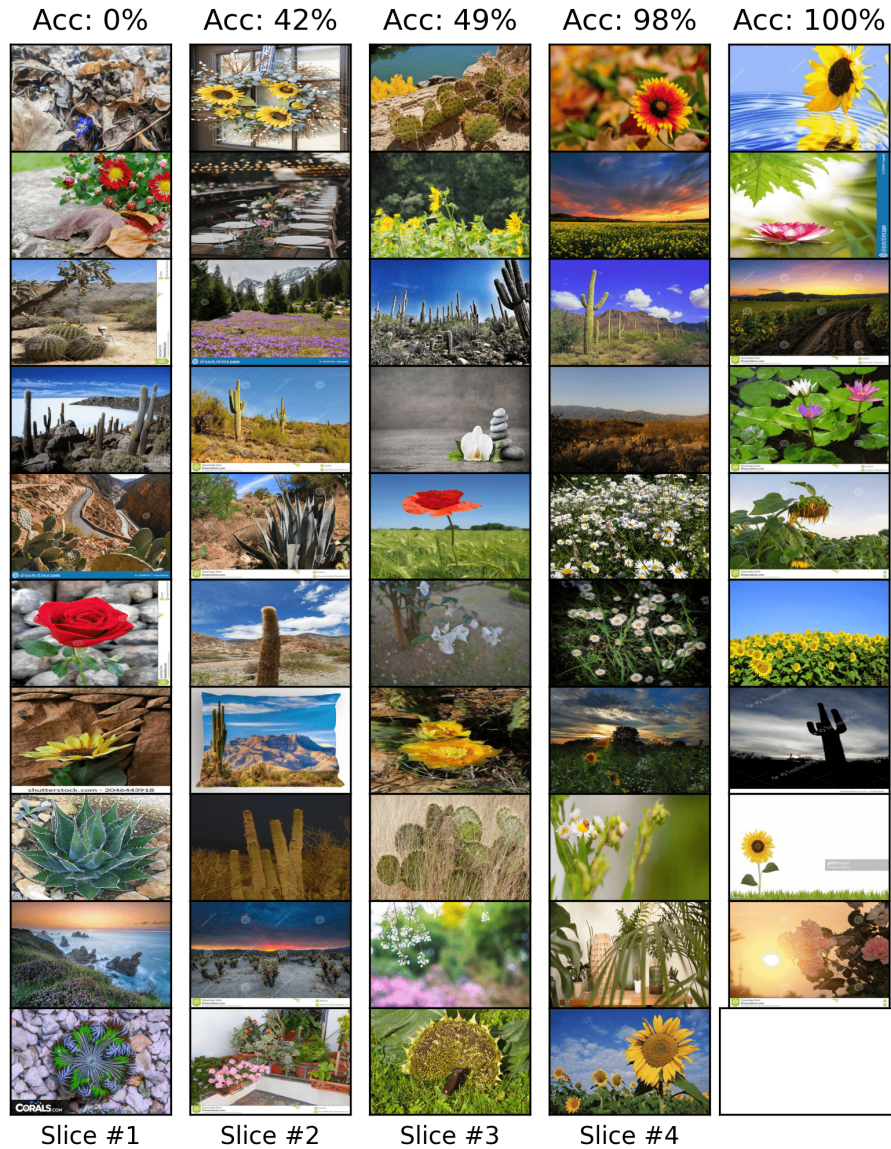


Fig. 17: Top-10 discovered images per slice for the *plants* class from NICO++⁹⁰ dataset. Note that the last slice corresponds to the slice: *dim lightning*, which is the dominant context (Context with largest number of samples for the *dim lightning* class in Table 4).

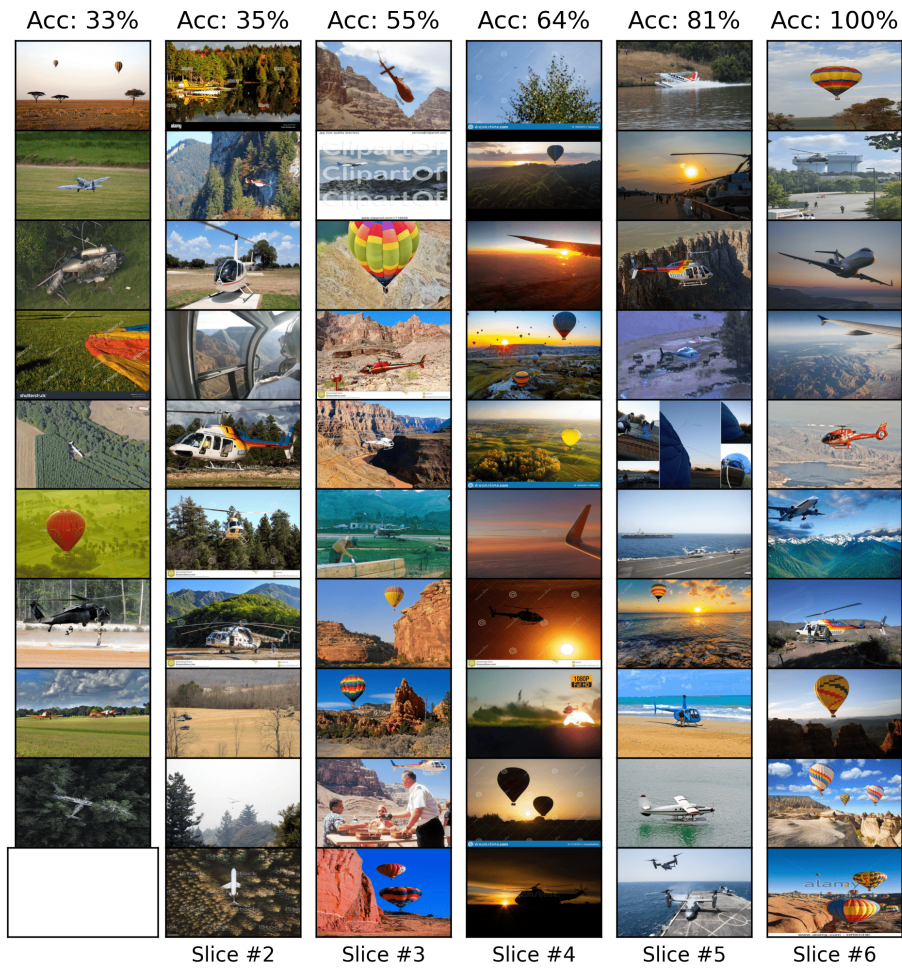


Fig. 18: Top-10 discovered images per slice for the *airways* class from NICO++⁹⁰ dataset. Note that the last slice corresponds to the slice: *outdoor*, which is the dominant context (Context with largest number of samples for the *outdoor* class in Table 4).

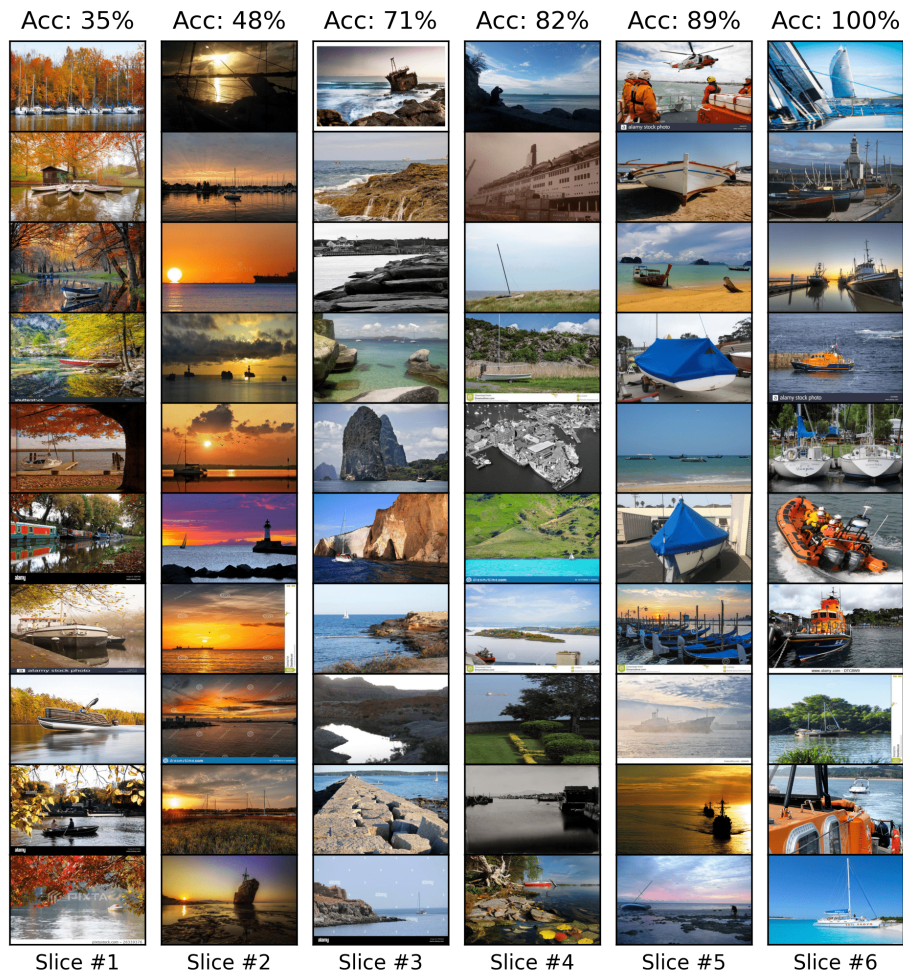


Fig. 19: Top-10 discovered images per slice for the *waterways* class from NICO++⁹⁰ dataset. Note that the last slice corresponds to the slice: *water*, which is the dominant context (Context with largest number of samples for the *water* class in Table 4).



Fig. 20: Top-10 discovered images per slice for the *landways* class from NICO++⁹⁰ dataset. Note that the last slice corresponds to the slice: *autumn*, which is the dominant context (Context with largest number of samples for the *autumn* class in Table 4).